Arabian Journal of Geosciences (2022) 15: 919
https://doi.org/10.1007/s12517-022-10171-w

ORIGINAL PAPER

Drought impact detection on wetlands in the arid area using Synthetic Aperture Radar data

Saeideh Maleki[1] · Vahid Rahdari[1] · Aireza Soffianain[2]

Received: 25 February 2022 / Accepted: 21 April 2022 / Published online: 4 May 2022

Abstract

Wetland conservation is crucial in arid areas on account of the high dependence of life on these ecosystems. Quantifying the effects of drought on wetlands is the initial step toward conservation action under drought condition. In this study, the ability of Synthetic Aperture Radar (TerraSAR-X and Sentinel 1 images) to detect the drought impacts on wetlands in arid areas was investigated. Synthetic Aperture Radar signals (SAR) acquired in dry and wet periods at two wavelengths (X-band ~ 3 cm, C-band ~ 6 cm), three polarizations (HH, VV, and VH), and three incidence angles (22°, 34°, and 53°) were applied. Primarily, the discrimination ability of each SAR data was assessed using the Transformed Divergence and Bhattacharyya Distance. The best image to create the wetland cover classes during wet and dry conditions was determined accordingly. The SAR images were classified employing the Support vector machine method and the classified images were assessed using n-folds cross-validation. Degradation in wetland cover classes as an index of drought-induced damage in the wetland was determined using a comparison between the flooded and dry conditions. Based on the findings of this paper, Sentinel-1 (C band) is of the ability to determine the degradation of wetland cover classes since it is capable of quantifying the increase in dead plants and bare lands. This study illustrated the potential of SAR data as a tool in arid land studies and could also promote the application of SAR data in wetland management. Free access to Sentinel-1 data and the 6-day overpass makes these data favorable images for wetland research.

Keywords Drought · Sentinel 1 · TerraSAR-X · Hamoun-e-Hirmand · Wetland

Introduction

Wetlands are valuable ecosystems that support biodiversity, regulate the water cycle, and decrease the negative effects of natural hazards, such as flooding (Hong et al. 2010). The role of wetlands is even more pivotal in arid areas where water scarcity is the most important limitation. Climate change, drought, human-induced changes, and water limitation over the recent years have led to widespread degradation in the wetlands of arid areas (Ye and Grimm 2013; Zhang et al. 2013; Zhao et al. 2016). Drought is a natural hazard that has affected a large part of the world (Minckley et al. 2013; Downard et al. 2014; Nikraftar et al. 2021). The vanishing of wetlands caused by drought has fiercely negative effects on local communities and wildlife (Saha et al. 2021; Hoque et al. 2020). People of such areas have to deal with various problems, including unemployment, poor harvesting, starving, immigration, and respiratory diseases caused by dust storms (Miri et al. 2019; Dikshit et al. 2022). Moreover, habitat loss due to water limitation threatens wildlife in these areas. Mitigation of drought risks necessitates a comprehensive drought management plan (Saha et al. 2021).

To protect all kinds of life against the negative effects of water limitation, the damages caused by drought should be investigated and estimated (Vicca et al. 2016). Narrow boundaries between the land cover types turn wetland mapping and investigation into a challenge (Gallant 2015). Thus, identification of the changes and harms in these ecosystems could be difficult (Klemas 2013; Gallant 2015; Hyde et al. 2006). An efficient tool for studying the changes in the wetlands is remote sensing (Zhang et al. 2013) since it provides

Responsible Editor: Biswajeet Pradhan

✉ Saeideh Maleki
smaleki@uoz.ac.ir

[1] Department of Environment, Faculty of Natural Resources, University of Zabol, Zabol, Iran

[2] Department of Environment, Faculty of Natural Resources, Isfahan University of Technology, Isfahan, Iran

accurate repeated data with spatial situation, which are useful for detection of the changes over dry period. These advantages make remote sensing an applicable tool for dynamic and vast area investigation. The drought impacts are always investigated by change in NDVI or other optical indices (Peng et al. 2011; Wang et al. 2015; Cunha et al. 2015). Meanwhile, owing to the advantages of SAR data, including penetration ability, sensitivity to soil and vegetation parameters, and its ability to provide data in all weather conditions, active remote sensing and SAR sensors have been widely utilized in recent wetland studies (Gallant 2015; Hyde et al. 2006; Klemas 2013; Touzi et al. 2007; Brisco et al. 2011). Toyra and Pietroniro (2005) mentioned that varying degrees of SAR penetrations are useful to detect the flooded area. White and Fennessy (2005) reported the water-saturated nature of the soil in wetlands to be effective in the high reflection of SAR transmitted energy. Additionally, several authors have emphasized both specular effects and double bounce scattering as beneficial characters of SAR data for wetland mapping (Bourgeau-Chavez et al. 2005). In fact, in SAR images, the specular effect results in the appearance of water as dark-colored patches, and double bounce scattering leads to the depiction of flooded vegetation as light-colored areas (Maleki et al. 2020). The contrast between the dark appearance of water and the light appearance of flooded vegetation ensures the optimal discrimination between land cover classes in wetlands (Grings et al. 2006; Henderson and Lewis 2008). However, SAR data are rarely applied in drought damage detection while the reduction in SAR backscatter in the dead plants due to the change in the water content of plants is valuable to map the effects of water limitation on plants (Corcione et al. 2016).

The necessity of conservation measures during drought periods further highlights the importance of applying appropriate data and methods for drought damage detection. This study used the advantages of SAR data to investigate drought impacts on Hamoun-e-Hirmand in Iran. Since SAR data are rarely used in arid areas, this research provided valuable information about the potential of SAR data to study drought impacts. The study area is a wetland dealing with prolonged drought which has led to degradation of different land cover classes. The degradation in the wetland cover in the dry period was assigned as an index of drought impact. The drought-associated impacts on the wetland were determined using the comparison between the wetland covers of flooded and dry conditions. This study provided further details on SAR data application and its results could be beneficial to future research on drought effects.

Study area and database

Study area

The study area was selected in Hamoun-e-Hirmand in the east of Iran, close to the Afghanistan boundary (Fig. 1); it was located between 30° 25′–31° 27′ E and 60° 56′–61° 43′ N. Previous studies have introduced Hamoun-e-Hirmand as the most important habitat for waterbirds' nesting and feeding in the east of Iran (Maleki et al. 2016; Behrouzirad 2009; Rahdari et al. 2012). Under normal conditions, the Hamoun ecosystem is fed by the Helmand River which raises from Afghanistan mountains. Nonetheless, this region is dealing with unprecedented drought which has caused a great crisis in the east of Iran. Over the recent years, due to the drought and the blockage of water flow by Afghanistan, Hamoun is dried out completely in a long period of the year. Poor harvesting, starving, and respiratory diseases caused by dust storms have put local communities through serious crisis (Shamohammadi and Maleki 2011; Beek and Meier 2006). On the other hand, local and migratory waterbirds have missed the only water resource in a vast desert. Meanwhile, before the drought, this ecosystem was the source of life; the Ramsar Convention introduced a large part of

Fig. 1 The study area in Hamoun-e-Hirmand in the east of Iran

Hamoun as a protected area, following which it was introduced as a world heritage (Ramsar 2016).

Field data

When Hamoun-e-Hirmand is flooded, three major wetland cover classes, namely open water, flooded vegetation, and bare lands, are formed (Maleki et al. 2016; Behrouzi-rad 2009; Rahdari et al. 2012). Figure 2 (a–c) presents this wetland in the wet period while Fig. 2 (d–f) illustrates it in the dry period. During the dry period, the plants dry out in a large part of the wetland and bare lands develop throughout the study area.

Field data were collected under both flooded and dry conditions of the wetland based on satellite overpass in 2019. All the samples were collected based on the stratified random sampling method. During the flooded period, 210 samples were collected from all the three wetland cover classes and the geolocation of each field observation was registered using the Global Positioning System (GPS). Taking into consideration the effect of the neighbor classes, all the data were collected in a homogeneous area. The characteristics of each sample, including vegetation type, vegetation cover percentage, and inundation condition, were recorded. These samples were re-evaluated under the drought conditions and the same data were recorded.

Satellite data

Since the majority of the plants in Hamoun-e-Hirmand are herbaceous, short-wavelength (X and C band) images were selected for this study. Considering the effects of incidence angle and polarization on the detection ability of SAR data, TerraSAR-X images at two incidence angles and Sentinel-1(S-1) images at two polarizations were applied (Table 1).

Methods

The degradation of wetland cover in the dry period is an index of drought-induced damage. Hence, in this paper, with the advantage of SAR data to detect the wetland cover classes in dry and flooded periods, the drought-induced damage in a wetland was estimated. To provide information about the SAR backscattering from wetland cover classes in the dry and flooded periods, the behavior of SAR data was first assessed under both dry and flooded conditions. Subsequently, the best image to separate the classes was tested

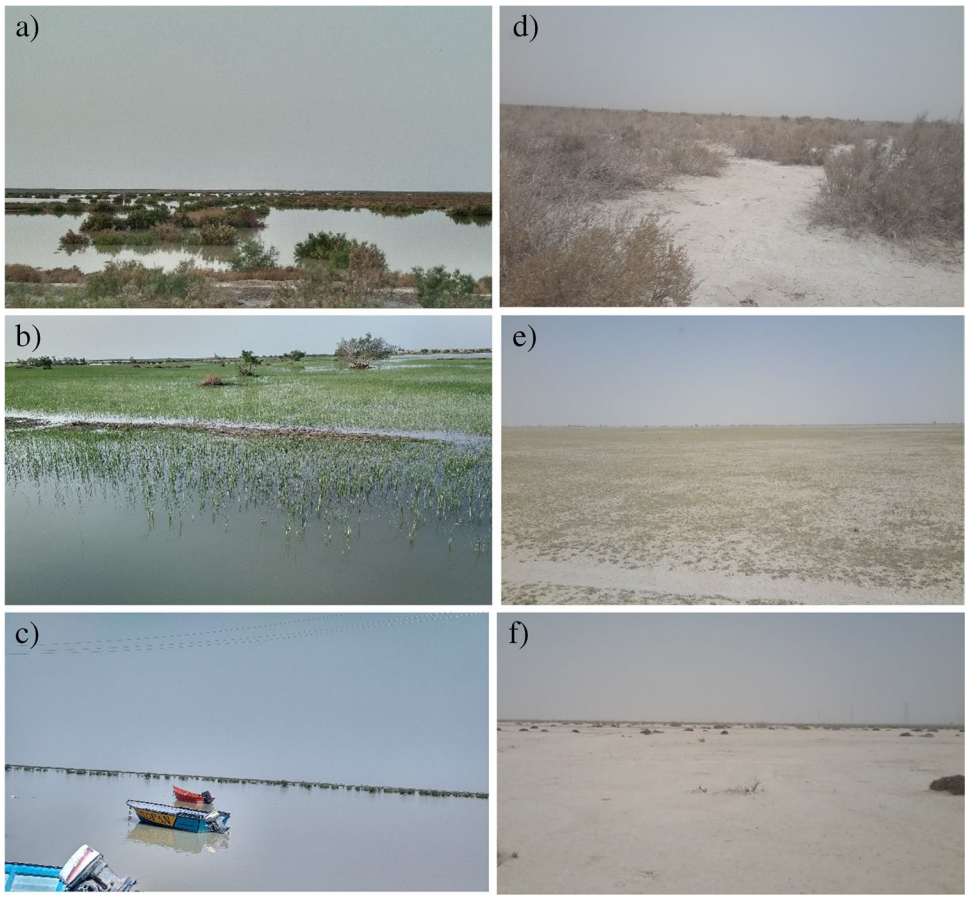

Fig. 2 The study area in flooded (**a**–**c**) and dry period (**d**–**f**)

Table 1 Satellite data used in this study

Date (dd/mm/yyyy)	Sensor	SAR incidence angle (°)	SAR polarization	Pixel spacing (m × m)	Wet/dry period
24/05/2019	S-1	34	VV, VH	10 × 10	Wet
19/05/2019	TerraSAR-X	53	HH	10 × 10	Wet
20/05/2019	TerraSAR-X	22	HH	10 × 10	Wet
11/11/2019	S-1	34	VV, VH	10 × 10	Dry
30/10/2019	TerraSAR-X	22	HH	10 × 10	Dry
01/10/2019	TerraSAR-X	53	HH	10 × 10	Dry

using TD and BD, and the wetland cover maps of dry and flooded conditions were created. The accuracy of the created maps was assessed with n-folds cross-validation. The decline in vegetation and water body were utilized as the index of drought-induced damage. These steps are described below.

Image preprocessing

SAR calibration was performed to calculate the real radar backscatter. Calibration is of great necessity for comparing SAR images to different characteristics (Niculescu et al. 2020). Orthorectification was then conducted to produce an image with topographical variations as close to real surface topography as possible (Small and Schubert 2008). Since speckles reduce the quality of SAR images, the Lee filter (5*5) was applied to minimize the speckle noise. The Sentinel Application Platform (SNAP) was used in the preprocessing steps.

Backscattering analysis

To provide complete information on the capability of C- and X-band to differentiate the changes in the wetland cover classes within the dry and flooded conditions, the backscattering of these bands was analyzed in both flooded and dry conditions. As mentioned in the "Field data" section, during the field surveys under the dry conditions, the location of each wetland cover class was registered. Using the field survey data, the polygons corresponding to each wetland cover class were generated. The mean backscattering of polygons for each class was calculated and the backscattering graph was created. Moreover, through the same method, SAR backscatters were analyzed under the flooded condition.

Separability analysis

TD and BD are used to investigate the separability between classes. The TD measure is a widely employed statistical separability criterion, which is simpler than the BD measure (Huang et al. 2016).

Both TD and BD separability measures are bounded between 0 and 2, where 0 shows no separability between the signatures of two classes, and 2 shows the complete separation. The larger the values, the better the final classification results (Dabboor et al. 2014). The following rules were mentioned by the previous literature for each range of separability values 'x':

$< \times < 1.0$ (very poor separability)
$< \times < 1.7$ (poor separability)
$1.7 < \times < 2.0$ (good separability)

The distance between the class means and the distribution of values from the means are used to calculate these measures that are provided by the covariance matrices of the classes (Ghoggali and Melgani 2009; Dabboor et al. 2014).

TD and BD measures are calculated as follows (Swain and Davis 1978; Dabboor et al. 2014; Huang et al. 2016):

TD

$$TD(i,j) = 2^{*}[1 - \exp(-D(i,j)/8)] \text{(Huangetal.2016)} \quad (1)$$

where:

- TD(i,j) = Transformed Divergence between classes i and j
- D(i,j) = divergence between classes i and j
- D(i,j) = 0.5*T[M(i)-M(j)]*[InvS(i) + InvS(j)]*[M(i)-M(j)] + 0.5*Trace[InvS(i)*S(j) + InvS(j)*S(i) -2*I]

where:

- M(i) = mean vector of class i, where the vector has Nchannel elements (Nchannel is the number of channels used)
- S(i) = covariance matrix for class i, which has Nchannel by Nchannel elements
- InvS(i) = inverse of matrix S(i)
- Trace[] = trace of matrix (sum of diagonal elements)
- T[] = transpose of matrix
- I = identity matrix

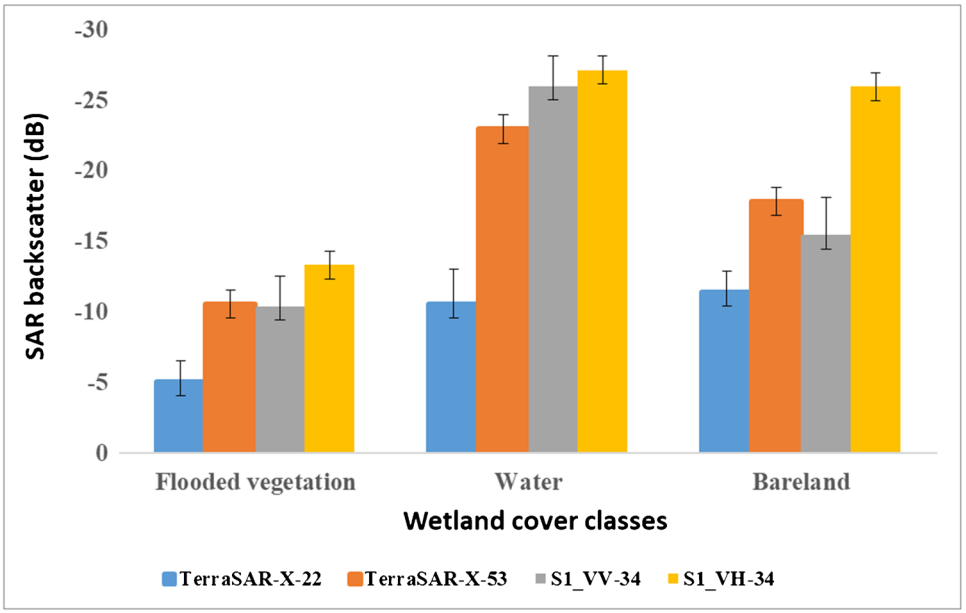

Fig. 3 The backscattering of TerraSAR-X and S-1 data over water, flooded vegetation and bare land in the flooded condition of wetland (Error bar = Standard deviation)

BD

$$BD(i,j) = 2^{*}[1 - \exp(-a(i,j))] \quad (2)$$

where:

- BD(i,j) = Bhattacharyya Distance between class i and j
- a(i,j) = 0.125*T[M(i)-M(j)]*Inv[A(i,j)]*[M(i)-M(j)] + 0.5 *ln{det(A(i,j))/SQRT[det(S(i))*det(S(j))]}

where:

- T, M, S, and Inv are as defined for TD measure
- A(i,j) = 0.5*[S(i) + S(j)]
- det() = determinant of a matrix
- ln{} = natural logarithm of scalar value
- SQRT[] = square root of scalar value

Image classification

Supervised classification method using Support vector machine (SVM) algorithm (Cortes and Vapnik 1995) was used to map the wetland covers. In this method, the training samples are employed to obtain a linear separating hyperplane in a multi-dimensional feature space. The SVM algorithm works based on minimizing the error risk and maximizing the margins between the separating hyperplane and the closest training samples (Bigdeli et al. 2013). In the SVM algorithm, the kernel function is applied as a nonlinear transformation of input data (Pal 2005; Pelletier et al. 2016; Bousbih et al. 2019). The wetland cover maps under the flooded and dry conditions were created. The classes with a higher accuracy were extracted from the results of TerraSAR-X-22°-53° and Sentinel 1-VV-VH classification and combined in order to create the wetland cover map. For the dry condition, Sentinel 1-VV-VH was applied.

Wetland cover classification accuracy assessment

Validation assures that the obtained classes have been correctly assigned to a wetland cover class (Bai et al. 2015). In this paper, fivefold cross-validation was applied to assess each image classification. The fivefold cross-validation method involves dividing the field samples into 5 folds, training the classification algorithm by 5–1 portions, and the remaining partition to evaluate the result. This process is repeated five times, each time using a different fold as the test set and the remaining partitions as the training data (Mccauley and Goetz 2004). Overall, Kappa and accuracy were applied to assess the accuracy of maps.

Wetland drought-induced damage detection

Using the post-classification method (Yadav and Ghosh 2019), the changes under the dry and flooded conditions were investigated. In this method, the wetland cover maps of both conditions, which have an acceptable accuracy, are overlaid. An acceptable level of accuracy, based on previous studies, has been defined as an accuracy higher than 80% (Kantakomar and Neelamsetti 2015(. The changes in each class within the flooded and dry periods were assigned as the drought-induced damage. The area of each wetland cover class was extracted from the created wetland cover maps

under the flooded and dry conditions. Then, the change rate for each class was calculated using Eq. (3).

$$\text{Change rate class X} = [\text{Class X area (flooded condition)} - \text{Class X area (dry condition)}]^{*}100 \quad (3)$$

Results

Backscattering analysis

Figure 3 illustrates the SAR backscattering of wetland cover classes. As seen, the highest backscattering belonged to the flooded vegetation in both C and X bands, including S1-VV and -VH, and TerraSARX -22° and 53° incidence angles, which is due to the double-bounce effect (Lang and Kasischke 2008). According to the comparisons between the backscattering of the wetland cover classes (flooded vegetation, open water, and bare lands), the water body has the lowest backscattering due to its smooth surface and the consequent specular reflection (Henderson and Lewis 2008). There is an insignificant difference between the backscattering of the water and bare lands in S-1-VH. Meanwhile, a significant difference was observed concerning VV polarization where the backscattering of the bare lands was 12 dB higher than that of water. In X-band, the backscattering of TerraSAR-X-53° from the bare lands was higher than that of water (9 dB).

Figure 4 represents the backscattering of TerraSAR-X and S-1 data over the green plants, dead plants, and bare lands when the wetland is dried out. As shown, although the green plants were not flooded and the wetland was dry, the S1-VH-VV and TerraSARX-22°-53° backscattering from the green plants were higher than those from the dead plants and bare lands. The highest backscatter from the green plants was achieved via S1-VV.

In both C and X wavelengths (S-1-VV-VH and TerraSARX-22° -53°), the backscattering from the bare lands was lower compared to that from the green and dead plants. The smoother surface of the bare lands compared to the surfaces covered by plants can justify this finding. As Aubert et al. (2011) mentioned, a minor part of the pulse that is transmitted to a smooth surface, returns to the sensor. Therefore, smooth areas appear in darker pixels rather than rough surfaces. The pixel value of these areas is generally below -20 dB (Baghdadi et al. 2008).

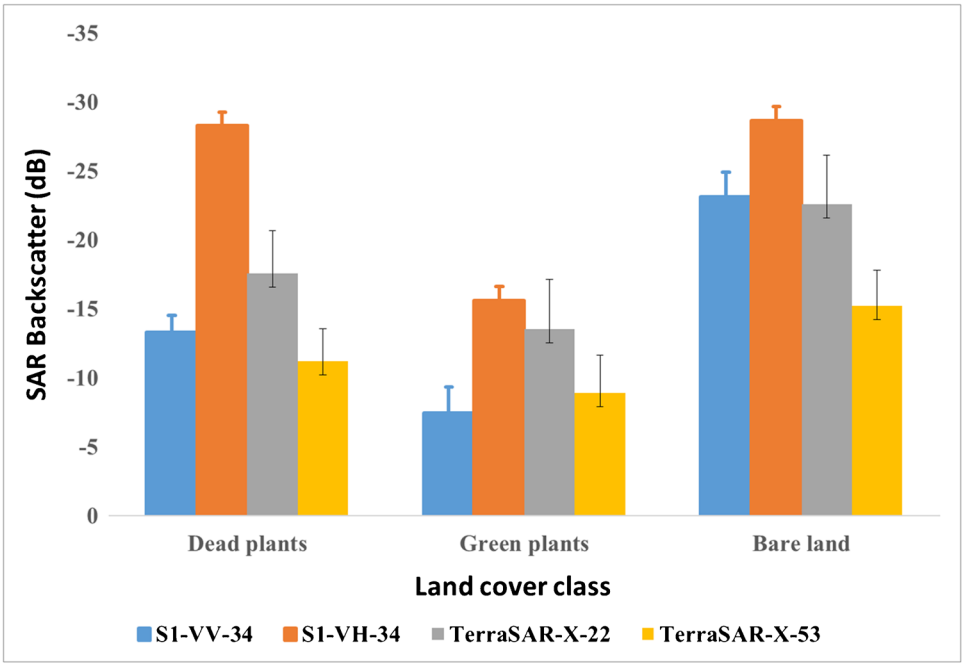

Fig. 4 The backscattering of TerraSAR-X and S-1 data over dead plants, green plants and bare land in the dry condition of wetland (Error bar = Standard deviation)

SAR discrimination ability

Figures 5 and 6 demonstrate the backscatter groups of the three wetland cover classes in the wet and dry periods, respectively. These figures were extracted from the polygons

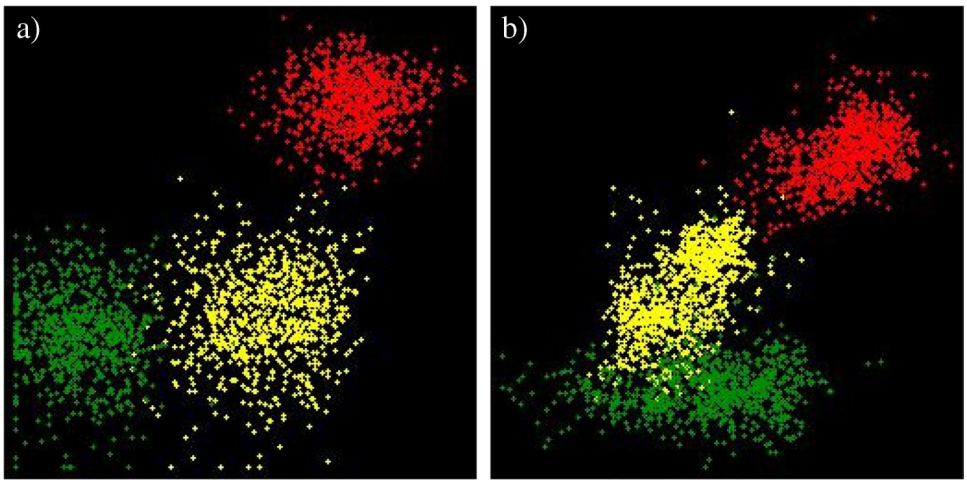

Fig. 5 The ability of (**a**) S-1 and (**b**)TerraSAR-X to separate the flooded plants from water and bare land in flooded period: green = water, yellow = bare-land, red = flooded plants

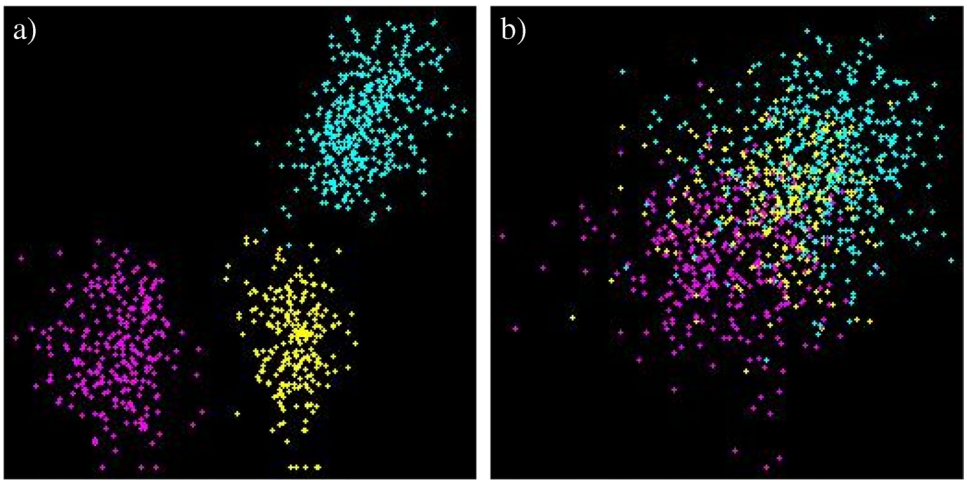

Fig. 6 The ability of (**a**) S-1 and (**b**) TerraSAR-X to separate the dryplants from bare land and green vegetation in dry period: pink = Bare land, yellow = dead plants, blue = green plants

drawn on each class based on the field surveys. Based on Fig. 5, the red group (flooded plants) did not overlap with the two other groups in both a (S-1) and b (TerraSAR-X) plots. Therefore, the flooded plants were separable from the bare lands and water with both S-1 and TerraSAR-X. The yellow (bare lands) and green groups (water) slightly overlapped in the S-1 plot, but in Terre-SAR-X, there was an overlap between these two groups. This overlap causes misclassification between water and bare lands. As Fig. 6 shows, in the dry period, the three groups, including pink (bare lands), yellow (dead plants), and blue (green plants), were completely separated with S-1. However, these groups showed a high overlap with Terra-SAR-X. This overlap leads to low accuracy for the separation of the wetland cover classes in the dry period.

Tables 2 and 3 show the results of TD and BD under the flooded conditions as the index of the separability of SAR data to discriminate between the wetland cover classes. In these tests, the TD or BD between 0.0 and 1.0 denote very poor separability, the TD or BD between 1.0 and 1.7

Table 2 Results of S-1, separability analysis in wet period (separability between class1 and class2)

Class1	Class2	Separability test	
		Bhattacharyya distance	Transformed divergence
Flooded vegetation	Water	1.99	1.99
	Bare land	1.97	1.98
Water	Flooded vegetation	1.99	1.99
	Bare land	1.81	1.83
Bare land	Flooded vegetation	1.97	1.98
	Water	1.81	1.83
Pair Separation (least to most)			
Water	and	Bare land	1.89
Flooded vegetation	and	Bare land	1.97
Flooded vegetation	and	Water	1.99

Table 3 Results of TerraSAR-X, separability analysis in wet period (Separability between class1 and class2)

Class1	Class2	Separability test	
		Bhattacharyya distance	Transformed divergence
Flooded vegetation	Water	1.99	1.99
	Bare land	1.89	1.91
Water	Flooded vegetation	1.99	1.99
	Bare land	1.44	1.61
Bare land	Flooded vegetation	1.89	1.91
	Water	1.44	1.61
Pair separation (least to most)			
Water	and	Bare land	1.44
Flooded vegetation	and	Bare land	1.89
Flooded vegetation	and	Water	1.99

illustrate poor separability, and TD or BD between 1.7 and 2.0 represent good separability between two classes. These statistics are commonly used for class separability calculations for hyperspectral and SAR data. Aubert et al. (2011) utilized TD and BD for evaluating the ability of TerraSAR-X SAR images to distinguish between bare soils, crops, and forests. Al-Ali (2011) investigated the separability of water bodies in the HH and VV channels of RADARSAT-2 and TerraSAR-X SAR via TD. Klein et al. (2004) calculated these statistics to test the separability of 10 wetland cover classes with Envisat advanced Synthetic Aperture Radar (ASAR) data.

Based on Table 2, the separation values between the flooded vegetation and both water and bare lands in C and X wavelengths (S-1-VV -VH and TerraSAR-X-22° -53°) were equal to or over "1.9". Thus, using these wavelengths, incidence angles, polarizations, along with flooded vegetation could be separated from water and bare lands. This finding is logical since plants are flooded and most of the energy of the transmitted pulse returns back to the sensor (double-bounce effect) (Kuenzer and Knauer, 2013). This leads to the appearance of very light pixels in the flooded vegetation area. On the other hand, the smooth surface of water and bare lands leads to the specular effect and dark pixels. In view of the differences between the backscattering of the flooded vegetation and those of the water and bare lands, the flooded vegetation became completely distinguishable in SAR images. This is the important advantage of SAR data, as also reported by studies on wetlands (Baghdadi et al. 2012; Dabrowska-Zielinska et al. 2014; Huang et al. 2014; Klemas 2013; Wilusz et al. 2017; Papa and Frappart 2021).

Table 4 Results of TerraSAR-X, separability analysis in dry period (Separability between class1 and class2)

Class1	Class2	Separability test	
		Bhattacharyya distance	Transformed divergence
Dead plants	Green plants	0.22	0.22
	Bare land	0.47	0.47
Green plants	Dead plants	0.22	0.22
	Bare land	0.98	0.98
Bare land	Dead plants	0.47	0.47
	Green plants	0.98	0.98
Pair separation (least to most)			
Dead plants	and	Green plants	0.22
Dead plants	and	Bare land	0.47
Green plants	and	Bare land	0.98

According to the separation values in Tables 2 and 3, to map the bare land and water body, S-1 is the best image for distinguishing between these two classes (separability = 1.89); in other words, using C-band, bare land and water body could be completely separated. Grady et al. (2014) mentioned the low ability of the L band in discriminating between water body and bare land. They concluded that the close backscattering of these two classes in the L band led to their misclassification. However, based on Table 2, S-1 is useful for the bare lands and water mapping.

The results of the TD and BD test under the dry condition are presented in Tables 4 and 5. Overall, under the dry condition, S-1 yielded better results than the X band and produced higher separability values for all the three classes (green plants, dead plants, and bare lands). It is hence possible to map green and dead plants and bare lands using S-1 images. The ability of SAR data to discriminate between green and dead plants is of particular importance in drought

Table 5 Results of S-1, separability analysis in dry period (Separability between class1 and class2)

Class1	Class2	Separability test	
		Bhattacharyya distance	Transformed divergence
Dead plants	Green plants	1.91	1.94
	Bare land	1.98	1.99
Green plants	Dead plants	1.91	1.94
	Bare land	1.99	1.99
Bare land	Dead plants	1.98	1.99
	Green plants	1.99	1.99
Pair separation (least to most)			
Dead plants	and	Green plants	1.91
Dead plants	and	Bare land	1.986771
Green plants	and	Bare land	1.999488

damage monitoring. In fact, accurate mapping of dead plants determines areas that suffer from drought.

Wetland cover mapping

Based on the results of backscattering analysis and separability tests under the flooded condition, both C and X bands are of benefit for mapping flooded vegetation, water, and bare lands (Antonova et al. 2016; Jia et al. 2013). Therefore, these images were classified using SVM, and the most accurate classes were selected to map the wetland cover classes under the flooded condition. Figure 7-a depicts the water body, green plants, and bare lands under the flooded condition of Hamoun-e-Hirmand wetland.

The accuracy of this map was assessed using fivefold cross-validation. Table 6 exhibits the results of the accuracy assessment. An overall accuracy of 87% and overall Kappa coefficient equal to 0.82 were achieved, which confirmed the accuracy of the created map. Based on Fig. 7-a, the flooded vegetation was well separated from both bare and water lands. The bare land and water body were also completely distinguished in this figure.

The wetland cover map under the dry condition is presented in Fig. 7-b. Table 6 demonstrates the results of fivefold cross-validation. An overall accuracy of 85% and Kappa coefficient of 0.80 implied the acceptable accuracy of this map. These results confirmed the ability of the C band to produce reliable wetland cover maps under the dry condition of the wetland and to determine the dead plants.

Detection of drought-induced damage to the wetland

The change in the area of the flooded vegetation and water was applied as an index to determine the drought-related degradation in the wetland. For this purpose, the area of each wetland cover class was extracted from the created wetland cover maps under the flooded and dry conditions and the change rate for each class was calculated (Table 7). As the change rates indicated, 66% of the flooded vegetation and all the water body was lost due to drought. Figure 8 illustrates the degradation in the wetland ecosystem during the dry condition. The reduction in green plants and vanishing water imposes critical limitations for all kinds of life in this ecosystem. In an area where life completely depends on water, the vanishing of water would lead to a widespread crisis.

Discussion

To provide information about the SAR backscattering from wetland cover classes in dry and flooded periods, the behavior of SAR data was assessed under both dry and flooded conditions. Since the majority of the plants in Hamoun-e-Hirmand are herbaceous, short-wavelength (X and C band) images were selected for this study.

The obtained results revealed that during the inundation period, the highest backscatter belonged to the flooded vegetation compared to the other two classes, which causes complete discrimination of flooded vegetation. On the other hand, the water body appeared as dark patches due to the lowest S-1 backscattering of water. The results showed a 12 dB backscattering difference between the water and bare lands in VV polarization, which results in better discrimination between these two classes using S-1-VV.

The SAR backscatter from the dead plants was lower than that of the green ones. Corcione et al. (2016) and Maleki et al. (2020) reported that a reduction in the water content of plants caused the lower SAR backscatter in the dead plants. A difference between the dead and green plants was 12 dB, achieved via S1-VH. The dead plants had a backscatter close to that of the bare lands in S1-VH, but the difference between the backscatter of these two classes was 10 dB in S1-VV.

The TerraSAR-X backscatter from the green and dead plants showed approximately similar backscattering coefficients. Thus, TerraSAR-X is not an appropriate image to separate green and dead plants. For this reason, TerraSAR-X could not be recommended for determination of the drought-induced damage.

The results of discrimination ability under the dry condition showed that S-1 yielded better results than the X band and produced higher separability values for all the three classes (green plants, dead plants, and bare lands). It is hence possible to map green and dead plants and bare lands using S-1 images. The ability of SAR data to discriminate between green and dead plants is particularly important in drought damage monitoring. In fact, accurate mapping of dead plants determines the areas suffering from drought.

The results of the TD and BD test confirmed the ability of the C band to map the wetland cover classes under both flooded and dry conditions. It would thus be possible to determine drought damages in the dry period through comparison between the wetland cover maps produced under dry and flooded conditions.

Based on the results of the backscattering analysis and separability test under the dry condition, the C band performed better than the X band in wetland cover mapping. The C band's capability of separating the dead plants was valuable for the purpose of this research and drought damage determination. Therefore, the S-1 image was applied to create the wetland cover map when Hamoun-e-Hirmand was dried out.

Comparison between the created maps under the flooded and dry conditions implied that a large part of vegetation vanished due to droughts. The water body was also dried out completely and the dead plants developed throughout the

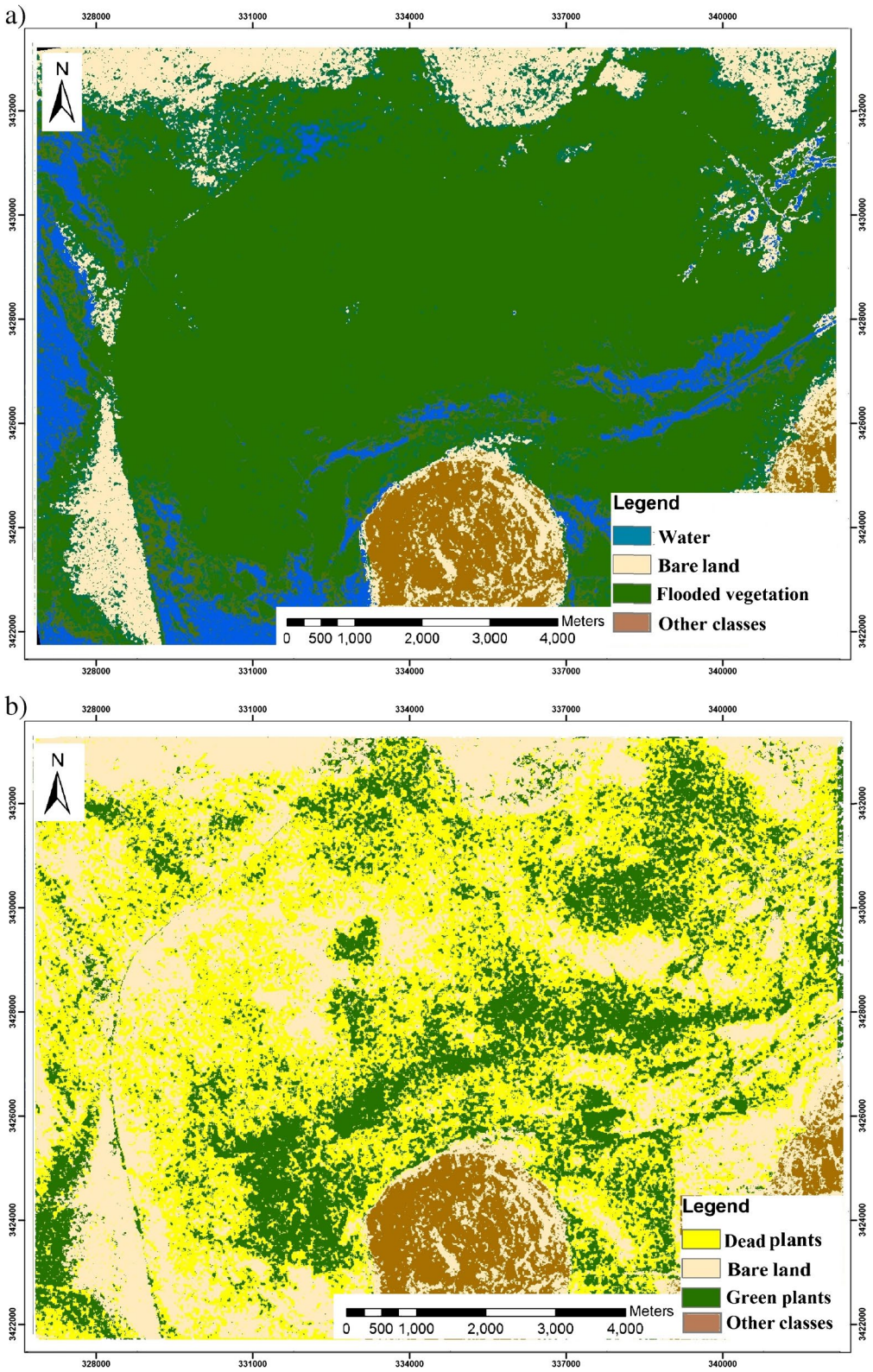

Fig. 7 Wetland cover map was produced using SAR images acquired in **a** the flooded condition, and **b** the dry condition

Table 6 Confusion matrices (%) for wetland cover map using (***a***) SAR images in the wet and (***b***) the dry periods

(*a*) Wetland cover class	Water	Flooded vegetation	Bare land	Total
Water	85.2	2.2	12.6	100
Flooded vegetation	7.3	89.2	3.5	100
Bare land	10.2	3.1	86.7	100
(*b*) Wetland cover class	Dead plants	Green plants	Bare land	Total
Dead plants	85.2	4.2	11.6	100
Green plants	5.7	86.9	7.4	100
Bare land	8.2	9.2	84.6	100

Table 7 The area of wetland cover classes (ha)

	Land cover area in flooded condition	Land cover area in dry condition	Change rate (%)
Green plants	6031.903	2018.31	−66.53
Dead plants	0	3837.96	+100
Water	575.115	0	−100
Bare land	1194.48	1944.18	+62.76

study area. Degradation of vegetation and the vanishing of water led to an increase in the bare land areas (Maleki et al. 2018). The created maps showed that although wetland was covered by green plants under the flooded condition, it experienced a widespread degradation under the dry condition due to drought. Since this wetland is the only water resource in an arid area, loss of water and green vegetation would cause widespread problems for both wildlife and the local population in the area (UNEP 2002; Debela et al. 2021). The wetland cover map under the dry condition confirmed this impending crisis and highlighted the parts of the wetland that needed emergency conservation measures to save life in the area.

As the change rates indicated, 66% of the flooded vegetation and all the water body was lost because of drought. Previous studies have identified the flooded vegetation in this area as the most valuable habitat for waterbirds (Maleki et al. 2016; Rahdari et al. 2012; Behrouzi-rad 2009). Nevertheless, 66% of the potential habitat of these birds was found to be degraded. Furthermore, since flooded vegetation serves as the source of forage for farm animals (Shamohammadi and Maleki, 2011), this degradation in flooded vegetation would lead to food shortage and poverty (Miri et al. 2019). The area of bare lands increased by 62% in the dry period, which is a widespread degradation triggered by drought.

Conclusion

In this paper, the effects of drought on wetland ecosystem were investigated using SAR data. Even though SAR data have been applied in several papers, they have not been commonly used in drought-concentrated studies. The ability of these data to separate green plants from dry ones and the potential of detecting vegetation, water, and bare lands is valuable in drought damage assessment. Since the penetration ability of smaller wavelengths is less than that of the L band, smaller wavelengths (the C and X bands) can detect the vegetation canopy even in a low density. Accordingly, the ability of C and X bands was applied in this study to detect the damages caused by drought. Furthermore, the effect of polarization and incidence angle was considered

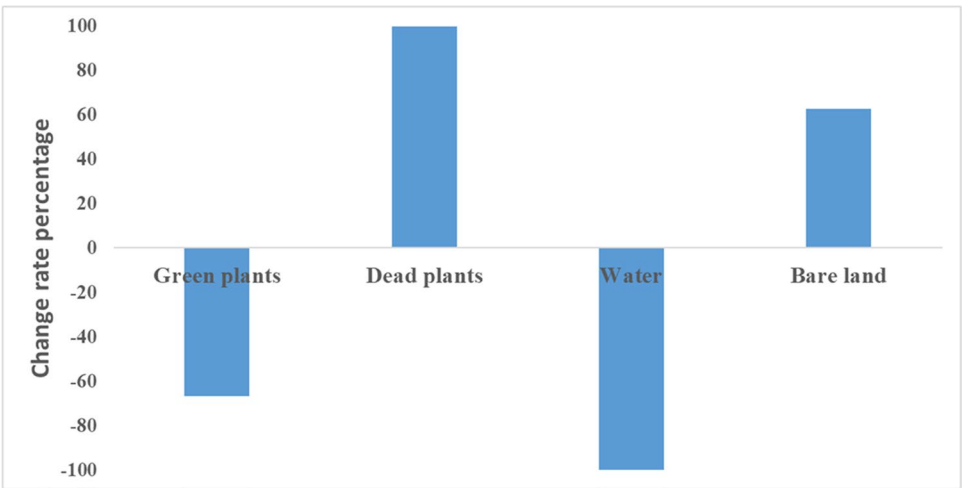

Fig. 8 Drought impacts on Hamoun-e-Hirmand

by applying three polarizations (HH, VV, and VH) and three incidence angles (22°, 34°, and 53°).

To determine the effect of drought, all the analyses were performed in wet and dry periods to compare the changes in the wetland covers between these two periods. The change in the area of wetland cover was applied as an index to determine the extent of drought-related degradation in the wetland. The area of change provides a quantitative index for destruction. The accuracy assessment of the image classification confirmed the usefulness of SAR data for wetland cover mapping. It shed light on the ability of SAR images to map wetland cover classes under both flooded and dry conditions.

According to the results of this study, S-1 had a complete configuration for the mapping of the bare lands and could discriminate between the dead and green vegetation under the dry condition. Given the importance of vegetation during the dry period in an arid area, it is essential to monitor dead and green plants for conservational objectives and S-1 images are a good choice for this purpose. As the backscattering of S-1 is very low in open water and high in flooded vegetation, these images could better differentiate between open water and flooded vegetation. Moreover, the double-bounce effect and specular scattering, as two important characteristics of SAR data, were found to be effective in satisfying the purpose of this research. The double-bounce effect in flooded vegetation and specular reflection of water provide contrast between classes. This contrast separates wetland cover classes with a higher accuracy, which turned SAR data into a favorable tool for mapping the plants in a wetland. These findings could be put in use as a reference in wetland studies.

Funding This paper was supported by University of Zabol (grant code: UOZ-GR-1348).

Declarations

Conflict of interest The authors declare that they have no conflict of interest with respect to this study and publication.

References

Al-Ali M (2011) Assessment of high resolution SAR imagery for mapping floodplain water bodies: a comparison between RADARSAT-2 and TerraSAR-X. Durham University, PhD diss.

Antonova S, Kaab A, Heim B, Langer M, Boike J (2016) Spatio-temporal variability of X-band radar backscatter and coherence over the Lena River Delta. Siberia Remote Sens Environ 182:169–191

Aubert M, Baghdadi B, Zribi M, Douaoui A, Loumagne C, Baup F, El Hajj M, Garrigues S (2011) Analysis of TerraSAR-X data sensitivity to bare soil moisture, roughness, composition and soil crust. Remote Sens Environ 115:1801–1810

Baghdadi N, Zribi M, Loumagne C, Ansart P, Anguela TP (2008) Analysis of TerraSAR-X data and their sensitivity to soil surface parameters over bare agricultural fields. Remote Sens Environ 112:4370–4379

Bai Y, Feng M, Jiang H, Wang J, Liu Y (2015) Validation of Land Cover Maps inChina Using a Sampling-based Labeling Approach. Remote Sens. 7(8):10589–10606

Baghdadi N, Cresson R, El Hajj M, Ludwig R, Jeunesse L (2012) Estimation of soil parameters over bare agriculture areas from C-band polarimetric SAR data using neural networks. Hydrol Earth Syst Sci 16:1608–1621

Beek E, Meier K (2006) Integrated water resources management for the Sistan closed inland delta, Iran. Delft, Netherlands: Delft Hydraulics

Behrouzi-rad B (2009) Waterbird populations during dry and wet years in the Hamoun Wetlands Complex. Podoces 4:88–99

Bigdeli B, Samadzadegan F, Reinartz P (2013) A multiple SVM system for classification of hyperspectral remote sensing data. J Indian Soc Remote Sens 41:763–776

Bousbih S, Zribi M, Pelletier C, Gorrab A, Lili-Chabaane Z, Baghdadi N, Ben Aissa N, Mougenot B (2019) Soil Texture Estimation Using Radar and Optical Data from Sentinel-1 and Sentinel-2. Remote Sens. 11(13):1520

Bourgeau-Chavez L, Smith K, Brunzell S, Kasischke E, Romanowicz B, Richardson C (2005) Remote monitoring of regional inundation patterns and hydroperiod in the Greater Everglades using Synthetic Aperture Radar. Wetlands 25:176–191

Brisco B, Kapfer M, Hirose M, Tedford B, Liu J (2011) Evaluation of C-band polarization diversity and polarimetry for wetland mapping. Can J Remote Sens 37:82–92

Corcione V, Nunziata L, Mascolo L, Migliaccio M (2016) A study of the use of COSMO-SkyMed SAR ping pong polarimetric mode for rice growth monitoring. Int J Remote Sens 37(3):633–647

Cortes C, Vapnik V (1995) Support-Vector Networks. Machine Learning 20:273–297

Cunha APM, Alvalá RC, Nobre CA, Carvalho MA (2015) Monitoring vegetative drought dynamics in the Brazilian semiarid region. Agric For Meteorol 214:494–505

Dabboor M, Howell S, Shokr M, Yackel J (2014) The Jeffries-Matusita distance for the case of complex Wishart distribution as a separability criterion for fully polarimetric SAR data. Int J Remote Sens 35(19):6859–6873

Dabrowska-Zielinska K, Budzynska M, Tomaszewska M, Bartold M, Gatkowska M, Malek I et al (2014) Monitoring wetlands ecosystems using ALOS PALSAR (L-Band, HV) supplemented by optical data: a case study of Biebrza wetlands in northeast Poland. Remote Sens 6:1605–1633

Debela MT, Wu Q, Li Z, Sun X, Omeno O, Li Y (2021) Habitat suitability assessment of wintering herbivorous anseriformes in Poyang Lake. China Diversity 13(4):171

Dikshit A, Pradhan B, Santosh M (2022) Artificial neural networks in drought prediction in the 21st century–a scientometric analysis. Appl Soft Comput 114:108080

Downard R, Endter-Wada J, Kettenring K (2014) Adaptive wetland management in an uncertain and changing arid environment. Ecol and Soci 19(2):23–39

Feng M, Jiang H, Wang J, Liu Y (2015) Validation of land cover maps in China using a sampling-based labeling approach. Remote Sens 7(8):10589–10606

Gallant A (2015) The challenges of remote monitoring of wetlands. Remote Sens 7:10938–10950

Grady D, Leblanc M, Bass A (2014) The use of radar satellite data from multiple incidence angles improves surface water mapping Rem. Sens. Environ. 140:652–664

Ghoggali N, Melgani F (2009) Automatic Ground-Truth Validation with Genetic Algorithms for Multispectral Image Classification. IEEE Trans Geosci Remote Sens IEEE TGEOSCI REMOTE 47(7):2172–2181

Grings FM, Ferrazzoli P, Jacobo-Berlles JC, Karszenbaum H, Tiffenberg J, Pratolongo P, Kandus P (2006) Monitoring flood condition in marshes using EM models and Envisat ASAR observations. IEEE Trans Geosci Remote Sens 44:936–942

Henderson FM, Lewis AJ (2008) Radar detection of wetland ecosystems: a review. Int J Remote Sens 29:5809–5835

Hong S, Wdowinski J, Kim S, Won S (2010) Multi-temporal monitoring of wetland water levels in the Florida Everglades using interferometric synthetic aperture radar (InSAR). Remote Sens Environ 114:2436–2447

Hoque MAA, Pradhan B, Ahmed N (2020) Assessing drought vulnerability using geospatial techniques in northwestern part of Bangladesh. Sci Total Environ 705:135957

Huang C, Peng Y, Lang M, Yeo IY, McCarty G (2014) Wetland inundation mapping and change monitoring using Landsat and airborne LiDAR data. Remote Sens Environ 141:231–242

Huang H, Roy D P, Boschetti L, Zhang H K, Yan L, Kumar S S, ..., Li J (2016) Separability analysis of Sentinel-2A Multi-Spectral Instrument (MSI) data for burned area discrimination. Remote Sens 8(10):873

Hyde P, Dubayah R, Walker W (2006) Mapping forest structure for wildlife habitat analysis. Remote Sens Environ 102:63–73

Jia M, Tong Y, Zhang Y, Chen Y (2013) Multitemporal radar backscattering measurement of wheat fields using multifrequency (L, S, C, and X) and full-polarization. Radio Sci 48:471–481

Kantakomar LN, Neelamsetti P (2015) Multi-temporal land use classification using hybrid approach. Egypt J Remote Sens 18(2):289–295

Klein D, A Moll, G Menz (2004) Land cover/use classification in a semiarid environment in East Africa using multi-temporal alternating polarization ENVISAT ASAR Data. ENVISAT & ERS Symposium, Salzburg, September 6–10

Klemas V (2013) Using remote sensing to select and monitor wetland restoration sites: an overview. J Coast Res 29:958–970

Kuenzer C, Knauer K (2013) Remote sensing of rice crop areas. Int J Remote Sens 34(6):2101–2139

Lang M, Kasischke E (2008) Using C-band synthetic aperture radar data to monitor forested wetland hydrology in Maryland's coastal plain, USA. IEEE Trans Geosci Remote Sens 64:535–547

Maleki S, Soffianian AR, Koupaei SS, Saatchi S, Pourmanafi S, Sheikholeslam F (2016) Habitat mapping as a tool for water birds conservation planning in an arid zone wetland: the case study Hamoun wetland. Ecol Eng 95:594–603

Maleki S, Soffianian AR, Koupaei SS, Pourmanafi S, Saatchi S (2018) Wetland restoration prioritizing, a tool to reduce negative effects of drought; an application of multicriteria-spatial decision support system (MC-SDSS). Ecol Eng 112:132–139

Maleki S, Baghdadi N, Soffianian A, El Hajj M, Rahdari V (2020) Analysis of multi-frequency and multi-polarization SAR data for wetland mapping in Hamoun-e-Hirmand wetland. Int J Remote Sens 41(6):2277–2302

McCauley S, Goetz SJ (2004) Mapping residential density patterns using multi-temporal Landsat data and a decision-tree classifier. Int J Remote Sens 25 (6) 1077–1094

Minckley TA, Turner TS, Weinstein SR (2013) The relevance of wetland conservation in arid regions: a re-examination of vanishing communities in the American Southwest. J Arid Environ 88:213–221

Miri A, Dragovich D, Dong Z (2019) Wind-borne sand mass flux in vegetated surfaces–wind tunnel experiments with live plants. CATENA 172:421–434

Niculescu S, Boissonnat B, Lardeux C, Roberts D, Hanganu J, Billey A, Doroftei M (2020) Synergy of high-resolution radar and optical images satellite for identification and mapping of wetland macrophytes on the Danube Delta. Remote Sens 12(14):2188

Nikraftar Z, Mostafaie A, Sadegh M, Afkueieh JH, Pradhan B (2021) Multi-type assessment of global droughts and teleconnections. Weather Clim Extremes 34:100402

Papa F, Frappart F (2021) Surface water storage in rivers and wetlands derived from satellite observations: a review of current advances and future opportunities for hydrological sciences. Remote Sens 13(20):4162

Pal M (2005) Random forest classifier for remote sensing classification. Int J Remote Sens. 26:217–222

Pelletier C, Valero S, Inglada J, Champion N, Dedieu G (2016) Assessing the robustness of Random Forests to map land cover with high resolution satellite image timeseries over large areas. Remote Sens Environ 187:156–168

Peng C, Ma Z, Lei X, Zhu Q, Chen H, Wang W, Zhou X (2011) A drought-induced pervasive increase in tree mortality across Canada's boreal forests. Nat Clim Change 1(9):467–471

Rahdari V, Maleki Najafabad S, Afsari KH, Abtin E, Pri H (2012) Change detection of Hmoun wild life refuge using RS & GIS. Remote sensing and GIS Journal. Iranian Remote. Sens GIS Soci 3(2):5970

Ramsar Convention Secretariat (2016) The list of wetlands of international importance

Saha S, Kundu B, Paul G C, Mukherjee K, Pradhan B, Dikshit A, ... Alamri AM (2021) Spatial assessment of drought vulnerability using fuzzy-analytical hierarchical process: a case study at the Indian state of Odisha. Geomat Nat Haz Risk 12(1):123–153

Shamohammadi Z, Maleki S (2011) The life of Hamun, Iran

Small D, Schubert A (2008) Guide to ASAR Geocoding, RSL-ASAR-GC-AD, Issue 1.0, March

Swain PH, Davis SM (1978) Remote Sensing: The quantitative approach. McGraw-Hill, New York

Touzi R, Deschamp B, Rother G (2007) Wetland characterization using polarimetric RADARSAT-2 capability. Can J Remote Sens 33(1):56–67

Toyra J, Pietroniro A (2005) Towards operational monitoring of a northern wetland using geomatics-based techniques. Remote Sens Environ 97:174–191

UNEP (2002) Sistan oasis parched by drought. In: /DEWP/GRID-Geneva U (ed). 11–21

Vicca S, Balzarolo M, Filella I, Granier A, Herbst M, Knohl A et al (2016) Remotely-sensed detection of effects of extreme droughts on gross primary production. Sci Rep 6:28269

Wang H, Ge Q, Dai J, Mao Z (2015) Geographical pattern in first bloom variability and its relation to temperature sensitivity in the USA and China. Int J Biometeorol 59:961–969

White D, Fennessy MS (2005) Modeling the suitability of wetland restoration potential at the watershed scale. Ecol Eng 24:359–377

Wilusz A, Zaitchik B, Anderson M, Hain C, Yilmaz M (2017) Monthly flooded area classification using low resolution SAR imagery in the Sudd wetland from 2007 to 2011. Remote Sens Environ 194:205–218

Yadav V, Ghosh SK (2019). Assessment and prediction of urban growth for a mega-city using CA-Markov model. Geocarto Int 1–33

Ye L, Grimm NB (2013) Modelling potential impacts of climate change on water and nitrate export from a mid-sized, semiarid watershed in the US Southwest. Clim Change 120:419–431

Zhao A, Zhu X, Liu X, Pan Y, Zuo D (2016) Impacts of land use change and climate variability on green and blue water resources in the Weihe River Basin of northwest China. CATENA 137:318–327

Zhang Y, Zhang S, Xia J, Hua D (2013) Temporal and spatial variation of themain water balance components in the three rivers source region, China from 1960 to 2000. Environ Earth Sci 64:973–983